Nanotechnology 17 (2006) 1128-1133

Effect of material anisotropy on the self-positioning of nanostructures

G P Nikishkov[1]‡, Y Nishidate[1], T Ohnishi[2] and P O Vaccaro[3]

[1] University of Aizu, Aizu-Wakamatsu 965-8580, Japan

[2] Konan University, Dept. of Applied Physics, Faculty of Science, Kobe 658-8501, Japan

[3] ATR Adaptive Communications Research Laboratories 2-2-2, Hikaridai, Kyoto 619-0288, Japan

Abstract. Experimental and numerical investigation of the effect of material anisotropy on the self-positioning of epitaxial nanostructures has been performed. The self-positioning occurs due to lattice mismatch between two epitaxial material layers (GaAs and $In_{0.2}Ga_{0.8}As$) of a hinge. Both materials have cubic crystal symmetry and possess anisotropic mechanical properties. Dependance of a hinge curvature radius on material orientation angle was obtained experimentally by creating self-positioning hinges with different angles between the hinge axis and material crystallographic axes. Same self-positioning structures were modeled by solving geometrically nonlinear problems with a help of the finite element method. Experimental and numerical values of the hinge curvature radius are in qualitative agreement. It is found that material anisotropy significantly affects a shape of self-positioning structures.

‡ Electronic mail: niki@u-aizu.ac.jp

1. Introduction

Complicated three-dimensional nanostructures can be created using a self-positioning phenomenon of multilayer epitaxial structures [1, 2]. During etching out the sacrificial layer, self-positioning takes place due to lattice mismatch between two or more epitaxial material layers. In order to estimate the curvature of self-positioning hinges and tubes [2], closed-form equations for isotropic materials [3, 4] or isotropic computational modeling [4] are employed. However, nanostructures created by molecular beam epitaxy, consist of monocrystal layers and possess material anisotropic properties. For example, in this paper we consider a bilayer hinge composed of GaAs and $In_{0.2}Ga_{0.8}As$ layers. These materials have cubic crystal symmetry. The elastic properties of cubic crystal materials are described by three constants in principal material axes [5] instead of two constants in arbitrary coordinate system for isotropic materials. Since epitaxial nanostructures are composed of monocrystal layers then it is necessary to take into account material anisotropy.

In this paper, the effect of material anisotropy on curvature of self-positioning nanostructures is investigated using experimental procedure and computational modeling. Experimental study is based on creating epitaxial hinged nanostructures with different orientation in respect to principal material axes. Measurements of the hinge curvature indicates that the self-positioning is considerably affected by material orientation. The measured values of the hinge curvature radius are characterized by a noticeable data scatter. Because of this scatter it is desirable to compare experimental data with computational results.

Computational modeling of anisotropic self-positioning structures is performed with the use of the finite element method. In this study, we suppose that strains are elastic and small but the deformation process is characterized by large rotations and large displacements. This makes the problem geometrically nonlinear. Finite element procedures for solution of geometrically nonlinear problems have been considered by Bathe [6], Criesfield [7] and Reddy [8]. Only structures consisting of isotropic materials are treated in the above publications. Here, a finite element procedure for solution of three-dimensional anisotropic geometrically nonlinear problems with large translational and rotational displacements and small strains is presented. The procedure is based on the updated Lagrangian formulation with co-rotational material coordinate systems at finite element integration points. Results of finite element solutions for self-positioning structures consisting of anisotropic materials with cubic crystal symmetry are in qualitative agreement with experimental data.

2. Experimental investigation

An experimental procedure for forming self-positioning hinged nanostructures has been developed by Vaccaro et al [2]. A schematic of a self-positioning hinged nanostructure is presented in Fig. 1. Material layers are formed using the molecular beam epitaxy

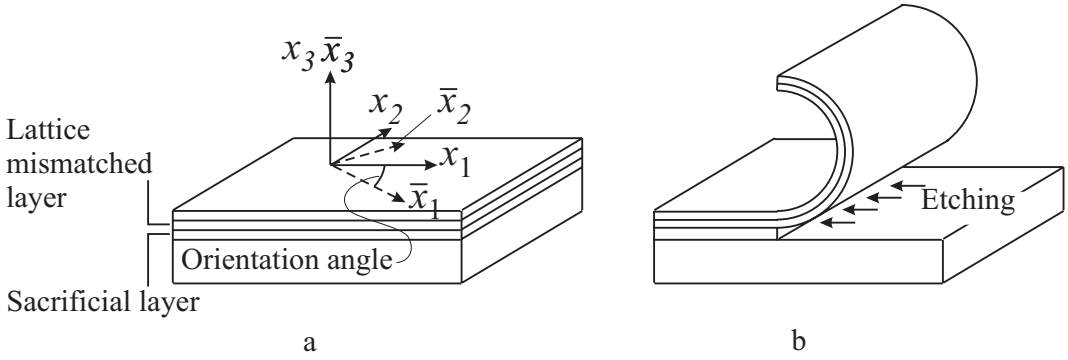

Figure 1. Self-positioning fabrication procedure: (a) multilayer structure, (b) self-positioning after etching out the sacrificial layer. The hinge orientation angle is an angle between the material axis $\bar{x}_1$ at time $t = 0$ and the global axis x_1.

method which builds a crystal structure on top of another structure with streams of molecules or atoms. The lattice period of the lattice-mismatched layer (lower strain layer) differs from that of the upper strain layer. If the lattice period of the upper strain layer is a and the lattice period of the lower strain layer is $a + \Delta a$ then the initial strain ε_0 exists in this layer: $\varepsilon_0 = \Delta a/a$.

A multilayer structure was grown by molecular beam epitaxy on a GaAs (100)-oriented substrate. Starting from the substrate, the structure consists of a GaAs buffer layer (400 nm), an $Al_{0.5}Ga_{0.5}As$/AlAs digital alloy (0.4 nm/0.4 nm × 50 periods = 39.2 nm) sacrificial layer, $In_{0.2}Ga_{0.8}As$ (56 nm) strained layer, a GaAs spacer layer (88 nm) an $Al_{0.5}Ga_{0.5}As$ (150 nm) selective etch layer, a GaAs (450 nm) plate layer, another $In_{0.2}Ga_{0.8}As$ (56 nm) strained layer and a GaAs (10 nm) cap layer. The top $In_{0.2}Ga_{0.8}As$ strained layer is included to balance the strain of the bottom $In_{0.2}Ga_{0.8}As$ layer and obtain flat micro-plates when the structures are released from the substrate. Fig. 2 shows the cross section of the multilayer structure.

After growth, devices were processed by photolithography and wet etching as shown in Fig. 3. The hinge region with the width 6 μm was defined by photolithography and the top layers were etched until reaching the $Al_{0.5}Ga_{0.5}As$ selective etch layer using the non-selective etching solution H_3PO_4:H_2O_2:H_2O (3:1:50). The remaining $Al_{0.5}Ga_{0.5}As$ was etched with the selective etching solution HF: H_2O (1:1), to stop at the GaAs spacer layer interface. The shape of the micro-plates was defined by another photolithography step and the epitaxial layers were etched down to the substrate, exposing the edge of the sacrificial layer. The sacrificial layer was selectively etched with HF:H_2O (1:6). At this time, the micro-plates moved up by themselves to the equilibrium position powered by the strain energy of the $In_{0.2}Ga_{0.8}As$ layer. The sample was soaked in pure water and dried using a method to prevent damage or sticking of the nanostructure due to surface tension of the water meniscus. The water was replaced by isopropyl alcohol, and this was replaced by tertiary butyl alcohol (liquid above 28°C). The sample was cooled until the alcohol solidified, and it was sublimated in a vacuum chamber.

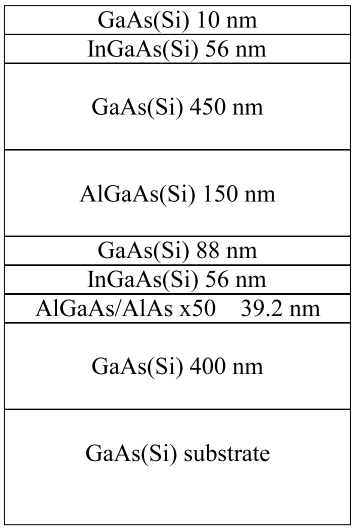

Figure 2. Cross section of the multilayer structure.

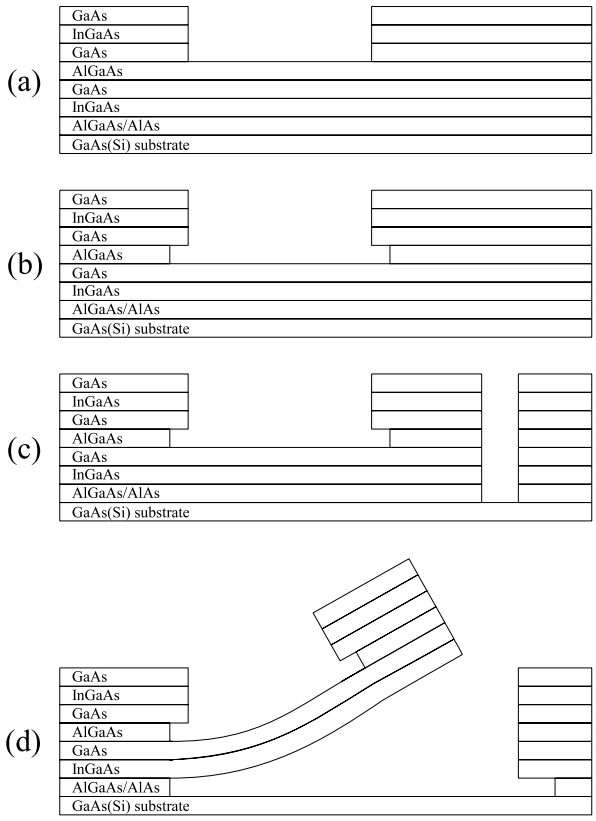

Figure 3. Multilayer structure processing: a) etch of the hinge until reaching the AlGaAs selective etch layer using the non-selective etching solution; b) the remaining AlGaAs on top of the hinge layers etched with the selective etching solution to stop at the GaAs spacer layer interface; c) Etch down to the substrate, exposing the edge of the sacrificial layer; d) sacrificial layer selectively etched and the micro-plate moves up to the equilibrium position.

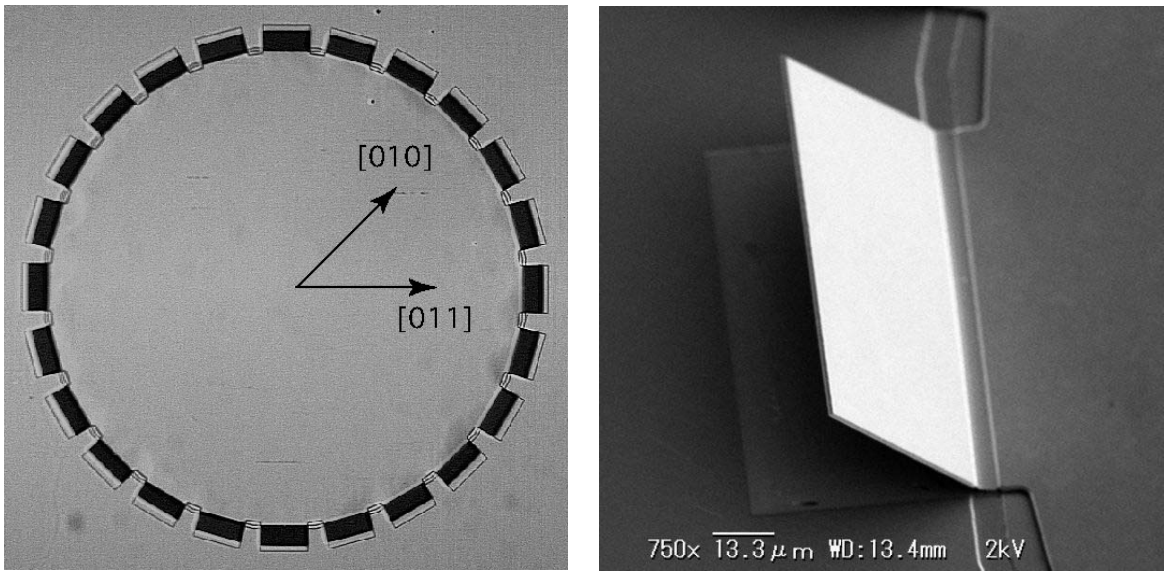

a b

Figure 4. Twenty four micro-plates with different hinge orientation (a); enlarged view of one micro-plate after self-positioning (b).

Fig. 4,a shows a SEM picture of the processed sample. Twenty four micro-plates with the width 100 μm and the length 50 μm are arranged in a circle, therefore hinge orientation changes 15 degrees for consecutive micro-plates. Fig. 4,b shows an enlarged view of one micro-plate.

In order to characterize relative orientation of the structure and the material, a global coordinate system $x_1,\ x_2,\ x_3$ and a material coordinate system $\bar{x}_1,\ \bar{x}_2,\ \bar{x}_3$ are employed. Both axes x_3 and $\bar{x}_3$ are normal to the structure surface at initial state. The global axis x_1 is along the hinge axis. The material axis $\bar{x}_1$ coincides with the [010] crystallographic axis. A hinge orientation angle is an angle between the material axis $\bar{x}_1$ at time $t = 0$ and the global axis x_1. Dependence of measured values of the plate elevation angle on material orientation angle is presented in Fig. 5.

The elevation angle of each plate was measured from the optical pictures of four circles of plates patterned in the same sample, including the one shown in Fig. 3,a. The dark squares are the standing plates. The brighter area adjacent to each square in the outside of the circle is the place where the plate rested before standing up. The dark-square width divided by the total width of the plate before standing up is the elevation-angle cosine. The curvature radius of the hinge was trigonometrically calculated from this angle and the hinge length (6 microns). The large dispersion of the experimental data is mainly due to unevenness in the hinge etching.

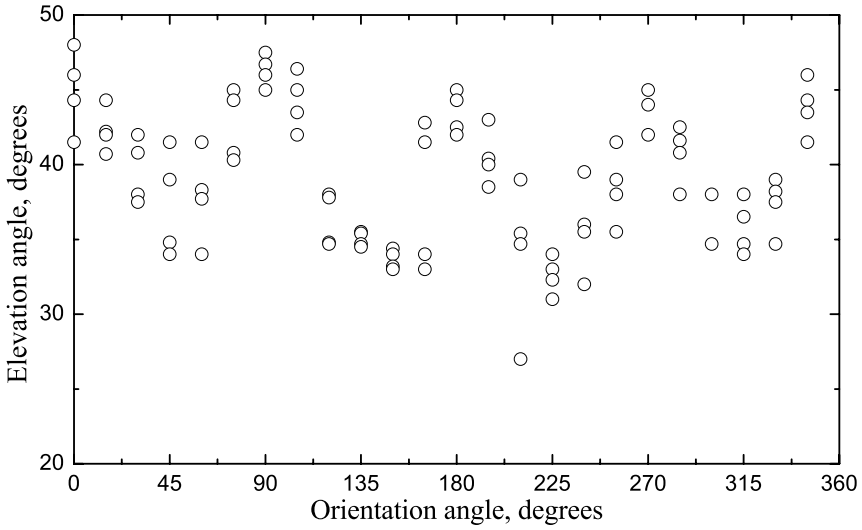

Figure 5. Experimental dependence of the plate elevation angle on the hinge orientation angle.

3. Finite element modeling

Here we present the finite element procedure for three-dimensional modeling of anisotropic elastic geometrically nonlinear structures under the influence of initial strains. It is assumed that rotations and translations are large but strains are small.

3.1. Coordinate systems

For derivation of finite element equations, we use tree coordinate systems (Fig. 6):

1) $x_1,\ x_2,\ x_3$ is the global cartesian coordinate system (fixed in space, used for the whole structure);
2) $\xi_1,\ \xi_2,\ \xi_3$ is the local element coordinate system (nonorthogonal, movable, one for each finite element);
3) $\bar{x}_1,\ \bar{x}_2,\ \bar{x}_3$ is the material coordinate system (orthogonal, movable, defined at any point inside a finite element).

The global coordinate system is employed in the global finite element equation system. The local coordinate systems are used for interpolation within finite elements. Material coordinate axes are involved in anisotropic constitutive relations. The material coordinate system can be introduced at any point of the structure. It rotates with the material in respect to the fixed global coordinate system.

We use three-dimensional isoparametric hexagonal elements for problem discretization. In such elements, nodal shape functions are used for geometry and field approxi-

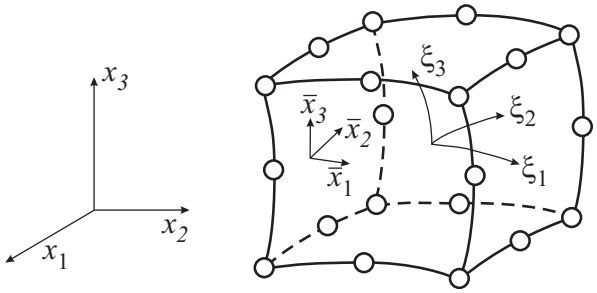

Figure 6. Global cartesian coordinate system $x_1,\ x_2,\ x_3$, local element coordinate system $\xi_1,\ \xi_2,\ \xi_3$ and material coordinate system $\bar{x}_1,\ \bar{x}_2,\ \bar{x}_3$.

mation:

$$\begin{aligned} x_i(\xi_1,\xi_2,\xi_3) &= N_m(\xi_1,\xi_2,\xi_3)x_i^m \ , \\ u_i(\xi_1,\xi_2,\xi_3) &= N_m(\xi_1,\xi_2,\xi_3)u_i^m \ . \end{aligned} \tag{1}$$

Here x_i are the global coordinates of the point with local coordinates $\xi_1,\ \xi_2,\ \xi_3$; x_i^m are the coordinates of the mth element node; u_i are the displacements; u_i^m are the displacements of the mth element node. In these relations and further in this paper, the repeated indices imply summation.

Since the local coordinate system ξ_i is not orthogonal, its axes cannot be used directly as axes of the material coordinate system. However, it is convenient to use local coordinates ξ_i for building the material coordinate system $\bar{x}_i$ at any point inside the finite element. Unit vectors $\vec{e}_{\xi_i}$ tangent to the local coordinates ξ_i have the following components in the global coordinate system:

$$\begin{aligned} \vec{v}_{\xi_i} &= \left\{ \frac{\partial x_1}{\partial \xi_i} \ \ \frac{\partial x_2}{\partial \xi_i} \ \ \frac{\partial x_3}{\partial \xi_i} \right\} \ , \\ \vec{e}_{\xi_i} &= \frac{\vec{v}_{\xi_i}}{|\vec{v}_{\xi_i}|}. \end{aligned} \tag{2}$$

Derivatives of the global coordinates in respect to local coordinates can be estimated using Eq. (1):

$$\frac{\partial x_j}{\partial \xi_i} = \frac{\partial N_m}{\partial \xi_i} x_j^m \ . \tag{3}$$

Let us adopt that the unit vector $\vec{e}_{\bar{x}_1}$ of the material coordinate $\bar{x}_1$ coincides with the direction of the unit vector $\vec{e}_{\xi_1}$ (tangent to the local coordinate ξ_1). Then two other unit vectors of the material coordinate system can be determined as vector products:

$$\begin{aligned} \vec{e}_{\bar{x}_1} &= \vec{e}_{\xi_1} \ , \\ \vec{e}_{\bar{x}_3} &= \vec{e}_{\xi_1} \times \vec{e}_{\xi_2} \ , \\ \vec{e}_{\bar{x}_2} &= \vec{e}_{\bar{x}_3} \times \vec{e}_{\bar{x}_1} \ . \end{aligned} \tag{4}$$

Direction cosines α_{ij} for transformations from the global coordinate system x_i to the material coordinate system $\bar{x}_i$ are expressed through the unit vectors $\vec{e}_{\bar{x}_1}$:

$$\alpha_{ij} = \cos(\bar{x}_i \ x_j) = e_{\bar{x}_i j} \ . \tag{5}$$

Transformations of vectors from the global coordinate system to the material coordinate system and back are performed in the following ways:

$$\begin{aligned} \bar{x}_i &= \alpha_{ij} x_j \ , \\ x_i &= \alpha_{ji} \bar{x}_j \ . \end{aligned} \tag{6}$$

3.2. Anisotropic constitutive law

Referring to a fixed orthogonal coordinate system, the stress tensor σ_{ij} and the strain tensor ε_{ij} for an anisotropic elastic material are related through the Hooke's law by

$$\sigma_{ij} = C_{ijkl} \varepsilon_{kl} \ . \tag{7}$$

The elasticity tensor C_{ijkl} contains 81 coefficients. Because of the symmetry of stress and strain tensors the elasticity tensor have the symmetry properties $C_{ijkl} = C_{jikl} = C_{ijlk}$, which allows to represent the Hooke's law in so-called contracted form using matrix-vector notations:

$$\begin{aligned} &\sigma = \mathbf{C} \varepsilon \ , \\ &\sigma = \{\sigma_{11} \ \ \sigma_{22} \ \ \sigma_{33} \ \ \sigma_{12} \ \ \sigma_{23} \ \ \sigma_{31}\} \ , \\ &\varepsilon = \{\varepsilon_{11} \ \ \varepsilon_{22} \ \ \varepsilon_{33} \ \ 2\varepsilon_{12} \ \ 2\varepsilon_{23} \ \ 2\varepsilon_{31}\} \ , \end{aligned} \tag{8}$$

where $\mathbf{C}$ is the contracted 6×6 elasticity matrix; σ, ε are the contracted 1×6 stress and strain vectors. The contracted form of the Hooke's law is convenient for using in a finite element computations since it reduces the number of array dimensions.

For triclinic crystal symmetry the elasticity matrix $\mathbf{C}$ is fully populated and symmetric thus having 21 independent components. Numerical modeling in this paper is performed for cubic crystals. The elasticity matrix for materials with cubic crystal symmetry has the following appearance:

$$\mathbf{C} = \begin{bmatrix} C_{11} & C_{12} & C_{12} & & & \\ C_{12} & C_{11} & C_{12} & & & \\ C_{12} & C_{12} & C_{11} & & & \\ & & & C_{44} & & \\ & & & & C_{44} & \\ & & & & & C_{44} \end{bmatrix} \tag{9}$$

Transformations from the global coordinate system to the material coordinate system for the stress and elasticity tensors are performed in the full tensor form:

$$\begin{aligned} \bar{\sigma}_{ij} &= \alpha_{ip} \alpha_{jq} \sigma_{pq} \ , \\ \bar{C}_{ijkl} &= \alpha_{ip} \alpha_{jq} \alpha_{kr} \alpha_{ls} C_{pqrs} \ . \end{aligned} \tag{10}$$

During calculations of element matrices and vectors, it is more efficient to use matrix-vector notation. Thus operations of contraction and expansion for the stress and elasticity tensors are necessary. To perform these operations it is useful to introduce two index vectors:

$$\begin{aligned} \mathbf{m} &= \{1 \ \ 2 \ \ 3 \ \ 1 \ \ 2 \ \ 3\} \ , \\ \mathbf{n} &= \{1 \ \ 2 \ \ 3 \ \ 2 \ \ 3 \ \ 1\} \ . \end{aligned} \tag{11}$$

Contraction from the stress tensor to the stress vector and expansion from the stress vector to the stress tensor are done as follows:

$$\begin{aligned} &\sigma_p = \sigma_{m_p n_p} , \qquad p = 1...6, \\ &\sigma_{m_p n_p} = \sigma_p , \qquad p = 1...6. \end{aligned} \tag{12}$$

The expansion operation should be accompanied by filling symmetrical terms of the stress tensor $\sigma_{ij} = \sigma_{ji}$. For the elasticity tensor, contraction and expansion operations are carried out in the following ways:

$$\begin{aligned} &C_{pq} = C_{m_p n_p m_q n_q} , \qquad p = 1...6, \qquad q = 1...6, \\ &C_{m_p n_p m_q n_q} = C_{pq} , \qquad p = 1...6, \qquad q = 1...6. \end{aligned} \tag{13}$$

To finish expansion of the elasticity tensor it is necessary to fill symmetric terms $C_{ijkl} = C_{jikl} = C_{ijlk}$.

3.3. Finite element equations

The incremental element equation relating load and displacement increments looks like follows:

$$^t\mathbf{k}\Delta\mathbf{u} = {}^{t+\Delta t}\mathbf{f} - {}^t\mathbf{r} . \tag{14}$$

Here $^t\mathbf{k}$ is the element tangent stiffness matrix at time t, $\Delta\mathbf{u}$ is the nodal displacement increment, $^{t+\Delta t}\mathbf{f}$ is the load vector at time $t + \Delta t$, and $^t\mathbf{r}$ is the vector of nodal internal forces that correspond to the current stress state at time t.

The element tangent stiffness matrix $\mathbf{k}$ is a sum of two matrices: the usual linear stiffness matrix $\mathbf{k}_e$ and the nonlinear addition $\mathbf{k}_\sigma$ depending on the stress state:

$$^t\mathbf{k} = {}^t\mathbf{k}_e + {}^t\mathbf{k}_\sigma . \tag{15}$$

A 3×3 block of the linear element stiffness matrix $\mathbf{k}_e$ corresponding to combination of nodes with local numbers m and n is calculated as follows:

$$(^t\mathbf{k}_e)^{mn} = \int\limits_{^tV} \mathbf{B}_m^T \mathbf{C} \mathbf{B}_n dV . \tag{16}$$

Here $\mathbf{B}_m$ is a 3×6 block of the displacement differentiation matrix containing derivatives of the shape function for node m; $\mathbf{C}$ is the contracted elasticity matrix in the global coordinate system. Integration is performed over the current element volume ^tV in the global coordinate system which is used to form a global finite element equation system. Coefficients of the nonlinear element stiffness matrix $\mathbf{k}_\sigma$ are equal to (this expression is given in index notation since it is simpler than that in matrix-vector form):

$$(^t k_\sigma)_{ij}^{mn} = \int\limits_{^tV} {}^t\sigma_{kl} \frac{\partial N_m}{\partial x_k} \frac{\partial N_n}{\partial x_l} \delta_{ij} dV . \tag{17}$$

Here m, n are local node numbers; i, j are indices related to the global coordinate axes (x_1, x_2, x_3); $^t\sigma_{kl}$ are stresses in the global coordinate system; $N_m = N_m(\xi_1, \xi_2, \xi_3)$ are

nodal shape functions and δ_{ij} is the Kronecker delta symbol. Stresses σ_{kl} are defined in the material coordinate system. Transformation from the material (integration point) coordinate system to the global coordinate system should be done prior to integration.

Vector $\mathbf{f}$ in Eq. (14) contains nodal equivalents of various loads applied to the finite element model. In this article, self-positioning due to lattice mismatch is considered. A nodal block of the fictitious force vector ${}^t\mathbf{f}$ for modeling of lattice mismatch with the initial strain ε_0 is computed as:

$$({}^t\mathbf{f})^m = \int\limits_{{}^tV} \mathbf{B}_m^T \mathbf{C} \boldsymbol{\varepsilon_0} dV \ . \tag{18}$$

where $\boldsymbol{\varepsilon_0} = \{\varepsilon_0 \quad \varepsilon_0 \quad \varepsilon_0 \quad 0 \quad 0 \quad 0\}$ is the initial strain vector. Nodal internal forces ${}^t\mathbf{r}$ are obtained by integration of stresses over the current element volume in the global coordinate system:

$$({}^tr)_i^m = \int\limits_{{}^tV} {}^t\sigma_{ik} \frac{\partial N_m}{\partial x_k} dV \ . \tag{19}$$

Element equations are assembled into a global equation system using element connectivity information:

$${}^t\mathbf{K}\boldsymbol{\Delta}\mathbf{U} = {}^{t+\Delta t}\mathbf{F} - {}^t\mathbf{R} \ , \tag{20}$$

where ${}^t\mathbf{K}$ is the global stiffness matrix at time t, $\boldsymbol{\Delta}\mathbf{U}$ is the nodal displacement increment, ${}^{t+\Delta t}\mathbf{F}$ is the nodal equivalent of the applied load at time $t + \Delta t$, and ${}^t\mathbf{R}$ is the vector of nodal internal forces corresponding to stresses at time t.

4. Results for anisotropic hinged structures

The finite element procedure for the solution of three-dimensional anisotropic geometrically nonlinear problems has been implemented as a C computer code. The 20-node hexahedral isoparametric element shown in Fig. 6 is used for discretization. The strains and the stresses are controlled at Gaussian integration points $2 \times 2 \times 2$ in the material coordinate frames. The initial strain ε_0 is divided into n increments. At each step an increment of the initial strain ε_0/n is applied, and the finite element equation (20) is solved. Coordinate update is performed at each iteration.

The hinged micro-plate used in computational modeling has the hinge of the size 6 μm along x_1 by 100 μm along x_2 (see Fig. 1,a). The top strain layer has a thickness t_1=88 nm. It is composed of GaAs with lattice constant a_1=0.56536 nm. The lower strain layer made of $In_{0.2}Ga_{0.8}As$ has the following thickness and lattice period: t_2=56 nm, a_2=0.57347 nm. The difference in lattice constants creates the initial strain in the lower strain layer: $\varepsilon_0 = (a_2 - a_1)/a_1 = 0.014345$. Both materials are anisotropic with cubic crystal symmetry. Elastic material constants C_{11}, C_{12} and C_{44} for GaAs and for $In_{0.2}Ga_{0.8}As$ are given in Table 1.

A finite element model for the hinged structure was generated by sweeping a plane with a two-dimensional mesh in the depth direction. A three-dimensional mesh for

Elastic constant	GaAs	$In_{0.2}Ga_{0.8}As$
C_{11}	119.00	111.88
C_{12}	53.40	51.80
C_{44}	59.60	55.58

Table 1. Elastic material properties (GPa).

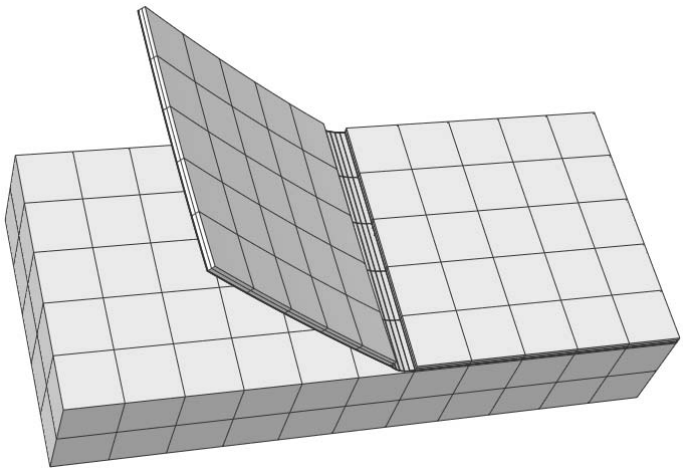

Figure 7. Final shapes of the hinged structure after self-positioning for zero hinge orientation angle.

the symmetrical half of the structure consists of 555 hexahedral 20-node elements and 3125 nodes. A series of problems for the self-positioning hinged nanostructure with different material orientations was considered. The hinge orientation is characterized by an angle between the material axis $\bar{x}_1$ at time $t = 0$ and the global axis x_1 (Fig. 1). It appeared that a calculated hinge curvature radius was of the order of the hinge width. The problems with high nonlinearity were solved by dividing the total initial strain into increments and by applying strain increments in a number of steps. Final shape of the nanostructure after its release from the substrate is shown in Fig. 7 for zero hinge orientation angle.

The curvature radius R of the hinge is estimated with the use of x_1- and x_3-coordinates of two points:

$$R = \frac{(x_1^B - x_1^A)^2 + (x_3^B - x_3^A)^2}{2(x_3^B - x_3^B)} \, .$$

Here x_1^B and x_3^B are horizontal and vertical coordinates of the point selected for the radius determination; x_1^A and x_3^A are coordinates of the hinge detachment from the substrate. Experimental values of the hinge curvature radius are determined from the micro-plate elevation angle (Fig. 5). The dependence of the hinge curvature radius R on the hinge orientation angle is presented in Fig. 8 where the values of R determined

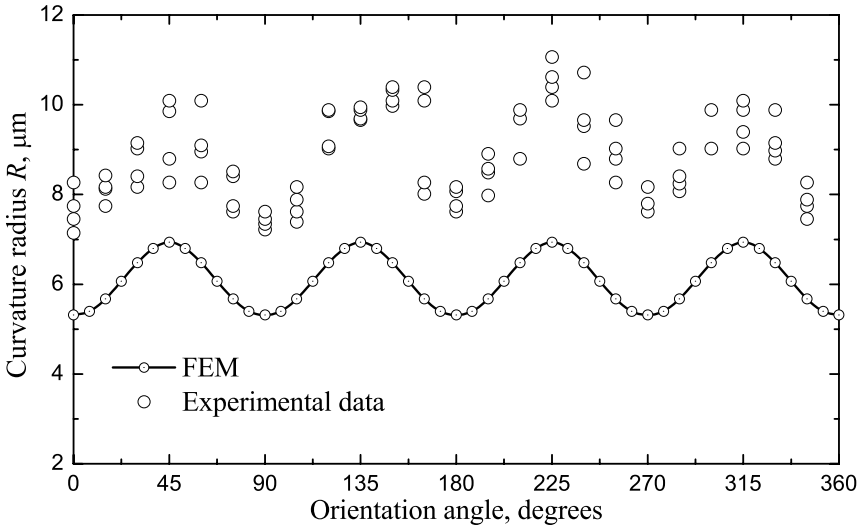

Figure 8. Dependence of the hinge curvature on the hinge orientation angle: comparison of finite element results with experimental data.

by the finite element method are compared with experimental data. It can be seen that the finite element results and experimental data have similar angular dependence. The ratio of maximum values to minimum values is about 1.3 for both numerical data and experimental data. However, absolute values obtained by computational modeling is about 30% lower than correspondent experimental values.

The difference between calculated and measured radius values may be related to partial stress relaxation in the $In_{0.2}Ga_{0.8}As$ layer due to formation of threading dislocations. The critical thickness for strain relaxation by generation of dislocations in $In_{0.2}Ga_{0.8}As$ epitaxial layers deposited on GaAs accordingly to the Matthews and Blackslee model [9] is 16 nm. The InGaAs thickness in our samples is 56 nm, much larger than this critical thickness. Samples with InGaAs thickness below the critical value would have been desirable, but unfortunately were not available. Therefore, we expect that the actual strain in the InGaAs layer is smaller than the strain calculated from the lattice mismatch. Goldman et al. [10] have shown that the residual strain in InGaAs layers above the critical thickness depends on epitaxial growth conditions and substrate characteristics. For example, $In_{0.13}Ga_{0.87}As$ layers of 250 nm thickness deposited on GaAs have a residual strain between 41% and 96% of the strain calculated from the lattice mismatch. Andrews et al [11] found a residual strain of about 30% of the calculated value in $In_{0.25}Ga_{0.75}As$ layers of 100 nm of thickness. The residual strain in our samples should be also considerable. Due to the partial relaxation of initial strain in our samples, experimental curvature radius is systematically larger than calculated one. It was not possible to model stress relaxation due to dislocations because dislocation dynamics is not in the scope of the finite element procedure. However, there is qualitative agreement in the dependence of the curvature radius on the orientation

angle.

5. Conclusion

Experimental technique and finite element modeling have been utilized to study effect of material anisotropy on self-positioning of hinged nanostructures consisting of GaAs and $In_{0.2}Ga_{0.8}As$ epitaxial layers.

In experimental research, hinged nanostructures with different hinge orientation angles were created using photolithography and selective wet etching. Computational modeling was performed by solution of anisotropic geometrically nonlinear problems with the help of the finite element method.

The finite element results for the hinge curvature radius are in qualitative agreement with experimental data. It is found that material anisotropy has significant influence on self-positioning of nanostructures. The ratio of maximum and minimum values of the curvature radius for the bi-layer GaAs-$In_{0.2}Ga_{0.8}As$ hinge with different material orientation is about 1.3. The effect of material anisotropy should be taken into account for estimation of self-positioning of epitaxial nanostructures.

References

[1] Golod S V, Prinz V Ya, Mashnov V I and Gutakovsky A K 2001 *Semicond. Sci. Technol.*, **16** 181
[2] Vaccaro P O, Kubota K and Aida T 2001 *Appl. Phys. Lett.*, **78** 2852
[3] Hsueh C-H 2001 *J. Appl. Phys.*, **91** 9652
[4] Nikishkov G P 2003 *J. Appl. Phys.*, **94** 5333
[5] Ting T C T 1996 *Anisotropic elasticity: theory and Applications* (Oxford: University Press)
[6] Bathe K-J 1996 *Finite Element Procedures* (Prentice-Hall)
[7] Criesfield M A 1996 *Non-Linear Finite Element Analysis of Solids and Structures. Volume 1: Essentials* (Wiley)
[8] Reddy J N 2004 *An Introduction to Nonlinear Finite Element Analysis* (Oxford: University Press)
[9] Matthews J W and Blakeslee A E 1974 *J. Cryst. Growth* **27** 118
[10] Goldman R S, Wieder H H, and Kavanagha K L 1995 *Appl. Phys. Lett.* **67** 344
[11] Andrews A M, Romanov A E, and Speck J S, Bobeth M and Pompe W, 2000 *Appl. Phys. Lett.* **77** 3740